3D Relativistic MHD Simulations of Pulsar Bow Shock Nebulae

Journal of Physics: Conference Series **1623** (2020) 012002 doi:10.1088/1742-6596/1623/1/012002

3D Relativistic MHD Simulations of Pulsar Bow Shock Nebulae

Niccolò Bucciantini[1,2,3], **Barbara Olmi**[1,2,3], **Luca Del Zanna**[2,1,3]

[1] INAF - Osservatorio Astrofisico di Arcetri, Largo E. Fermi 5, I-50125 Firenze, Italy
[2] Dipartimento di Fisica e Astronomia, Università degli Studi di Firenze, Via G. Sansone 1, I-50019 Sesto F. no (Firenze), Italy
[3] INFN - Sezione di Firenze, Via G. Sansone 1, I-50019 Sesto F. no (Firenze), Italy

E-mail: niccolo@arcetri.inaf.it

Abstract. Pulsars out of their parent SNR directly interact with the ISM producing so called Bow-Shock Pulsar Wind Nebulae, the relativistic equivalents of the heliosphere/heliotail system. These have been directly observed from Radio to X-ray, and are found also associated to TeV halos, with a large variety of morphologies. They offer a unique environment where the pulsar wind can be studied by modelling its interaction with the surrounding ambient medium, in a fashion that is different/complementary from the canonical Plerions. These systems have also been suggested as the possible origin of the positron excess detected by AMS and PAMELA, in contrast to dark matter. I will present results from 3D Relativistic MHD simulations of such nebulae. On top of these simulations we computed the expected emission signatures, the properties of high energy particle escape, the role of current sheets in channeling cosmic rays, the level of turbulence and magnetic amplification, and how they depend on the wind structure and magnetisation.

1. Introduction

Pulsar Wind Nebulae (PWNe) are synchrotron emitting sources powered by the wind of a pulsar (PSR). Usually, they are observed inside the supernova remnant (SNR) of their parent progenitor, but for old pulsars they can also form as a consequence of the direct interaction of the pulsar wind with the interstellar medium (ISM) [1–3]. Pulsar winds are ultra-relativistic outflows, with typical Lorentz factors in the range $10^4 - 10^7$, magnetised, and cold [4–6]. They are supposed to be mainly composed by electron-positron pairs [7–15]. The interaction with the ambient medium, forces these supersonic winds to slow down in a a strong termination shock (TS). It is there that particles are likely accelerated to a non-thermal distribution [16–19]. The observed non-thermal radiation is produced via synchrotron and inverse Compton scattering, arising from the interaction of these particles with the magnetic field in the nebula and with the background photon field.

Given that between 10% and 50% of all the pulsars are born with kick-velocity of the order of $100-500$ km s^{-1} [20–23], while the supernova remnant expansion is decelerated [24–27], they are fated to escape the supernova remnant shell on timescales of the order of a few tens of thousands of years. At this point their associated nebulae acquire a cometary-like shape due to the ram pressure balance between the pulsar wind and the surrounding incoming ISM (in the reference frame of the PSR) [28–30]. The pulsar is now located in the head of these nebulae and an

elongated tail forms that extends in the direction opposite to the pulsar motion. These objects are known as bow shock PWNe (BSPWNe). The formation of these systems was confirmed by numerical simulations in different regimes [30–33].

In the last years BSPWNe have been observed at many different wavelengths, with a large, and sometimes unexpected, variety of structures at different scales: different shapes and elongation of the tails, different morphologies in the bow shock head, different polarisation properties, hard X-ray outflows misaligned with the pulsar velocity [34–61]. Interestingly extended TeV halos have also been detected around BSPWNe [62]. Given that these nebulae could be one of the major contributors of leptonic anti-matter in the Galaxy, in competition with possible dark matter sources [63, 64], understanding the escape of particles from these systems, could have important consequences. Contamination from neutral hydrogen can also modify the dynamics and morphology of the bow-shock tail, as predicted by theoretical model and verified numerically [65–67].

Beginning with analytical and semi-analytical works [28, 29, 68], dating back to more than one decade, the first numerical models have been presented in the non-relativistic hydrodynamical regime by [30, 69], and in relativistic hydrodynamics and magneto hydrodynamics with spin-kick alinement by [31]. However there is no reason to assume spin-kick alignment, and to cope with the relative inclination one needs to work in full 3D. The third dimension is particularly important to correctly capture the structure of the magnetic field configuration [70], and in the study of the development of turbulence, which can be strongly affected by geometric constraints. The first 3D models of BSPWNe were presented by [32] but limited to the classical HD regime. Only recently 3D MHD simulations have been presented in the correct relativistic regime [33, 71–73]. More recently [74, 75], using a simplified, axisymmetric laminar semi-analytic model tuned on numerical simulations, have investigated for then first time how different magnetic field geometry act on the observed non-thermal synchrotron emission and polarisation, and on the propagation of high energy particles, showing the role played by current sheets and current layers.

Here we present the result of a detailed study of the dynamics, emission, and particle propagation properties of BSPWNe, done using 3D relativistic MHD simulations [72–76]. Various configurations were considered in terms of inclinations of the magnetic field with respect to the pulsar spin-axis, wind magnetisation, pulsar wind energy distribution, particle acceleration properties, in order to have a sample as complete as possible of the interaction conditions.

2. Numerical Setup and Simulations

Our simulations were done with the numerical code PLUTO [77, 78]. PLUTO is a shock-capturing, finite-volume code for hyperbolic and parabolic partial differential equations. Simulations were done with adaptive mesh refinement (AMR), corresponding to an effective resolution of 2048^3 cells at the highest level, sufficient to capture simultaneously the pulsar wind injection region and the large scale of the cometary tail of the nebula. A second order Runge-Kutta time integrator and an HLLD Riemann solver (the Harten-Lax-van Leer for discontinuities, [79, 80]) have been used, in order to better treat shear layers in the nebula. The relativistic pulsar wind is cold $p/\rho c^2 \approx 0.01$, and has a Lorentz factor $\gamma = 10$, high enough to ensure the correct relativistic regime. The outer medium is modelled as a cold incoming flow both with and without magnetic field. Solutions were computed for various relative inclinations, magnetisations σ, and pulsar wind energy distributions, making sure that the dynamics was relaxed to a quasi-steady regime. For a more detailed description of the setup and of the models we refer the reader to [72, 73, 76], where they are discussed and presented in more details. Please nota that the density and magnetic field can be scaled arbitrarily as far as the ratio, $B^2/\rho c^2$, is fixed.

The typical scale-length of these nebulae is the so called is the stand-off distance, where the

wind ram pressure equilibrates the ISM ram pressure:

$$d_o = \sqrt{\frac{\dot{E}}{4\pi c \rho_{\rm ISM} v_{\rm PSR}^2}} \tag{1}$$

where $\dot{E}$ is the pulsar spin-down luminosity, taken equal to the pulsar wind power, $\rho_{\rm ISM}$ is the ISM density, $v_{\rm PSR}$ the speed of the pulsar with respect to the local medium.

To summarise the main model parameters are:

- The pulsar is rest at the origin in the Cartesian coordinates, while the ISM has the velocity, $(0, 0, -v_{\rm PSR}) = (0, 0, -0.1c)$, along the z-axis.
- The pulsar spin axis lies in the $y - z$ plane and is offset by ϕ_M (the spin-kick inclination) from the z-axis.
- The pulsar wind is injected steadily from $r = 0.2d_o$ either with an isotropic energy distribution (cases I) or following the split-monopole prescription (cases A).
- The magnetic field injected with the pulsar wind and has only toroidal component with respect to the spin axis, while the one in the ISM lies in the $y - z$ plane.

The magnetisation is defined as $\sigma = B_o^2/(4\pi\rho_o\gamma^2c^2)$ where, B_o is the strength of the magnetic field in the equatorial plane of the wind at a distance $r = 0.2d_o$ (for a split monopole solution), and ρ_o is the wind density at the same location [81].

In computing emission maps, the 3D structure of the velocity and magnetic field is provided by our 3D relativistic MHD models. We assume, following [82], that the emitting pairs are distributed according to a power-law in energy, given the typical high flow speed found in numerical simulations, even X-ray emitting particles are only marginally affected by cooling [31], such that our results can reasonably apply even to higher energies. For simplicity we assume that the power-law index is uniform in the nebula. For the emitting particle density we adopt two different choices: either a uniform distribution, as was done in [75], or a density proportional to the local value of the thermal pressure, as it is customary in other PWNe models. In a few cases we have also investigated a third possibility that the emission is concentrated in the current sheets that form in the BSPWN. We build all of our maps using a spectral index $\alpha = 0$. This was shown by [75] to be a good average for the observed radio spectra, and changes in the typical observed range do not affect much the results. The polarised fraction is always given in terms of the theoretical maximum, that is 0.7 for $\alpha = 0$. Emission maps where computed for all simulations. Emissivity toward the observer is computed taking into account all relativistic effects, including Doppler boosting and aberration. For a complete description of the method used and the formalism adopted we refer to [82–85]. We have also computed the polarisation properties, accounting for relativistic polarisation angle swing.

In computing particles escape, given that we are interested in the escape from the very head of these nebulae, as in [75], particles that move backward at a distance exceeding $10-20d_o$, from the PSR are assumed to be lost in the tail. It is still likely that those particles can escape from the tail, but given that the tail might be in general more turbulent than the head, we expect the escape there to be more isotropic. Moreover, we assume that all high energy particles are injected from the PSR (or equivalently the pulsar wind) in the radial direction. The electric field is given by the ideal MHD condition $\mathbf{E} = -\mathbf{V}\times\mathbf{B}/c$ where $\mathbf{V}$ and $\mathbf{B}$ are the flow speed and magnetic field given by our RMHD simulations. All particles are injected with the same Lorentz factor, and we have investigated four cases with $\gamma = [0.5, 1.0, 3.0, 10.] \times 10^7$, corresponding to values where we expect the transition from Larmor radii in the magnetic field smaller than the size of the bow-shock set by its stand-off distance d_o, to larger than d_o. Particle trajectories in the electric

and magnetic fields of this system are computed using an explicit Boris Pushing technique [86–88], which ensures energy and phase space number conservation in the non-radiative regime. We verified, by computing radiative losses, that they are always negligible.

3. Dynamics

We summarise here the results of our numerical study on the dynamics, morphology, and magnetic field structure in BSPWNe. More details can be found in [72].

Comparing 3D with 2D HD runs we find a good agreement for isotropic winds, especially at intermediate values of the magnetisation ($\sigma = 0.1$). This is unexpected, since in principle one would expect a larger similarity in the low magnetisation cases. However for values of the magnetisation $\sigma < 0.1$ the dynamics is completely dominated by turbulence on small scales. On the other hand for larger values, the conditions at injection become dominant. In the tail it is quite clear the difference in the development of the local turbulence and in the level of mixing of the fluid, as shown in Fig. 1.

In the direction aligned with the pulsar motion ($z-$direction) the velocity structure shows a lower velocity channel around the z axis ($\sim 0.65c$ in 2D and $\sim 0.7 - 0.8c$ in 3D) surrounded by an higher velocity flow layer (with $\sim 0.85c$ in 2D and up to $0.9c$ in 3D). In the A cases the effect of turbulence is even more pronounced: injection matters only for $\sigma > 0.1$, and the typical structures in the tail remain coherent on shorter scales than in the corresponding I case. There is also a higher level of mixing between the pulsar wind and ISM material.

In the I cases the initial magnetic field configuration, and the current sheets separating field of opposite polarities, survive in the tail, while in the A ones turbulent mixing tends to destroy them even at higher magnetisation. We found that there is no efficient turbulent magnetic field amplification: in the presence of turbulence it tends just to reach equipartition with the turbulent kinetic energy, which is usually smaller than the thermal energy in the tail. In 3D there is evidence of magnetic field enhancement near to the contact discontinuity (CD), possibly the effect of an efficient shear instability amplification acting at the CD.

The forward shock shape is almost the same, the only exception being the A cases with the spin-kick inclination $\phi_M = \pi/4$: differences appear as small extrusions and blobs, possibly resulting as periodic perturbation of the forward shock. Fluctuations of the flow in the interior are not characterised by high values of the magnetic field, density or pressure. Moreover they arise on very small spatial scales, possibly making it difficult to be revealed by actual instruments due to resolution limits.

Major differences among various cases are visible mainly in terms of collimation or broadness of the tails, arising as the effect of different magnetic inclination and especially of the wind anisotropy. The average flow pattern in the tail between 2D and 3D runs is not significantly different (differences are largely in the head due to inclination and anisotropy). In the low σ regime there is a strongly turbulent magnetic field structure, suggesting that perhaps a laminar model is not likely to fully capture the magnetic field. For higher values of the magnetisation σ, the magnetic field is more coherent, qualitatively in agreement with the prediction of simplified laminar models [74].

4. Emission

We summarise here the results of our numerical study on the emission and polarisation properties of BSPWNe. More details can be found in [72].

Using our numerical simulations we analysed both cases of isotropic (I) and anisotropic (A) winds. In the case of uniform injection and high magnetisation, we found a strong correlation between the conditions at injection, as the inclination ϕ_M, and the surface brightness of our simulated maps. The trend in general agrees with that of fully laminar semi-analytic models [74]. There is a variety of morphologies, from systems brighter in the head to ones dominated

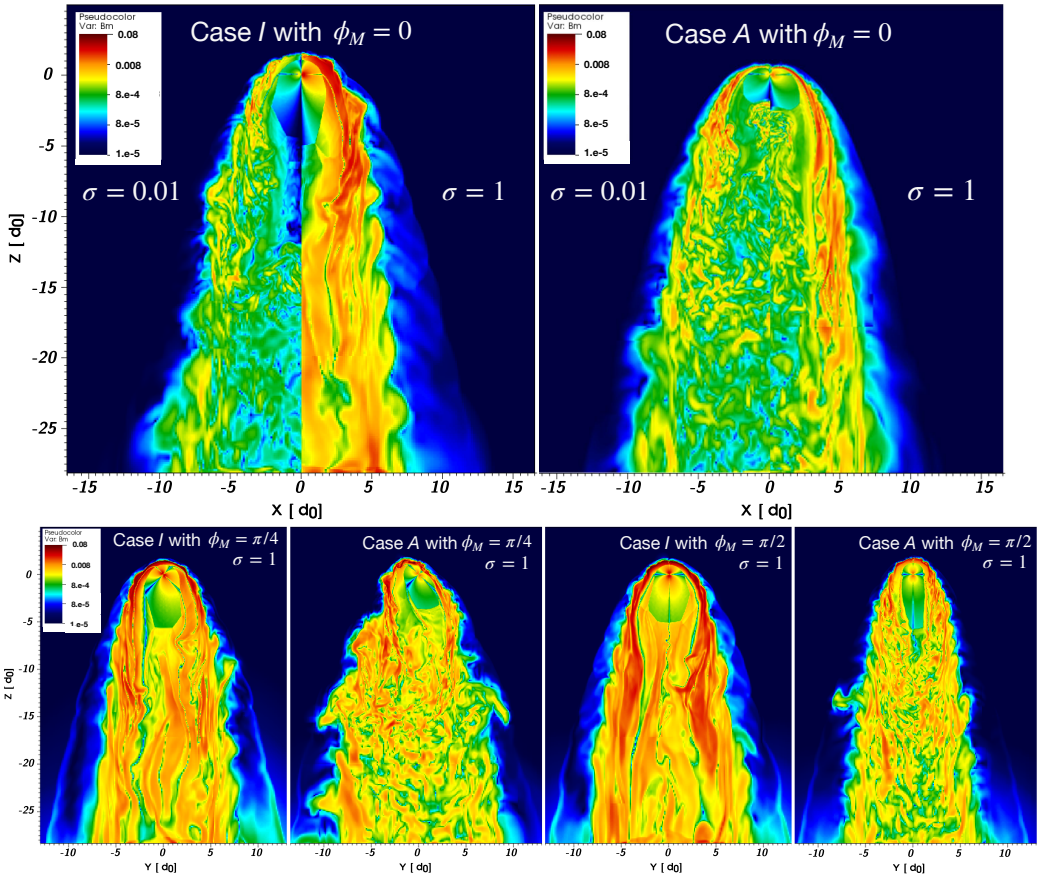

Figure 1. Map of the magnetic field strength in the $y = 0$ plane (in code units), normalised to the maximal nominal value. Upper panels: comparison for runs I (on the left) and A (on the right), for in cases where the pulsar spin-axis is aligned to its kick velocity; maps are composed by two halves of different value of magnetisation, lower on the left-side and higher on the right-side, respectively. Bottom panels: maps of the magnetic field strength for magnetisation $\sigma = 1.0$ and for the all the remaining inclinations ϕ_M, both for I and A cases. From [72].

by the tail. Some maps show bright wings. In computing the maps one needs also to consider the viewing angle χ, however the dependence on it of the observed properties is less marked and appreciable only at high resolution. In the high σ regime the polarised fraction is quite high in the tail. Once the magnetisation drops, turbulence begins to dominate the appearance of the maps, and it is far more difficult to find defined observational patterns. In this cases it will be hard to distinguish between different inclinations ϕ_M in a robust way.

Interestingly in our maps, apart from the strongly turbulent cases, we do not observe major time variations along the tail direction. This implies that time variability and temporal changes in the flow pattern are weak, and unlikely to give rise to major observational changes. On the other hand, changes in the polarisation properties of a BSPWN could likely point to a strongly anisotropic energy injection, and spin axis misalignment.

Our models were computed according to different scalings for the emitting particles density. If we consider a scaling proportional to the local pressure, typical of particles accelerated at the wind termination shock and then advected in the nebula, we find that the head is much brighter than the tail, even by a factor 10. Only in systems dominated by turbulence this difference is less enhanced. Indeed system like the Mouse nebula show a very bright head and a fainter tail,

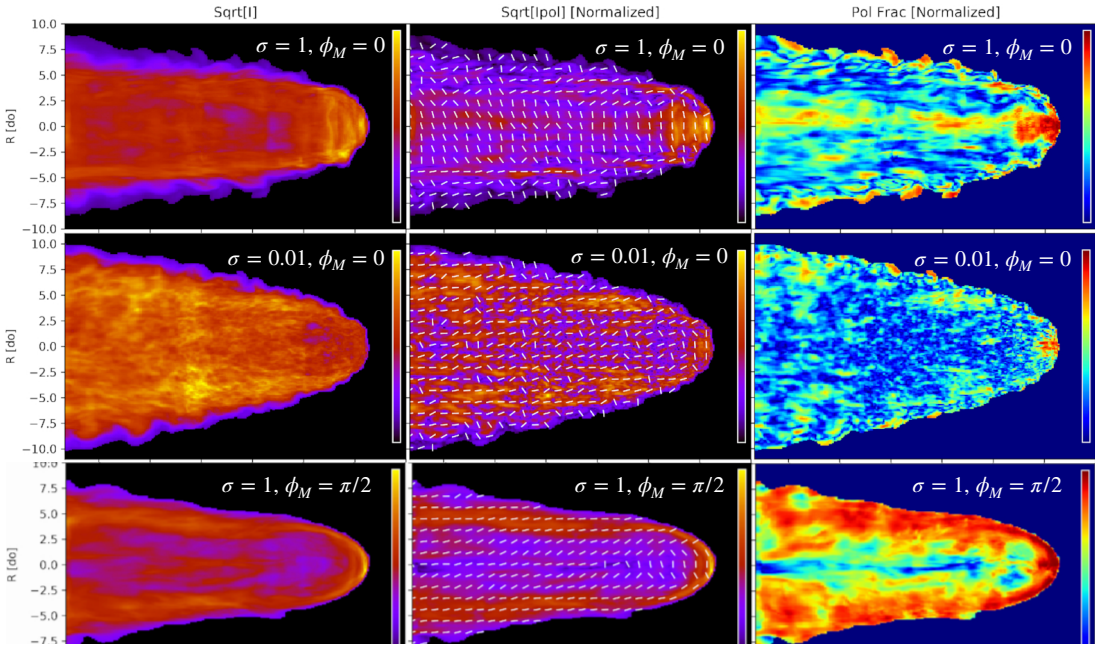

Figure 2. Emission maps for the case of a uniform wind with pulsar spin-axis aligned with the kick velocity and high magnetisation (upper row); the same but for low magnetisation (middle row), and finally for a pulsar spin-axis orthogonal to the pulsar the kick velocity again at high magnetisation (bottom row; viewed from the pulsar axis direction). All cases are computed assuming uniform local emissivity. From left to right: square root of the total synchrotron intensity normalised to the maximum, square root of the polarised intensity normalised to the maximum superimposed with the polarised direction, and polarised fraction normalised to the theoretical maximum for a power-law synchrotron with $\alpha = 0$. The colour scale is linear between zero and one. From [73].

but in many others there is no evidence for such brightness difference [36, 46]. This could be the signature of an acceleration process diffused in the bulk of the nebula. We also tried an emissivity scaled according to the strength of the currents, aiming at modelling the effect of reconnection and dissipation of currents. However there seem to be no appreciable difference with respect to a uniform emissivity.

In almost all cases the direction of the polarisation (the inferred direction of the magnetic field) seems to be almost aligned with the tail. This is an interesting aspect, most likely due to polarisation swing associated to the relativistic flow in the tail. If one suppresses relativistic beaming and aberration, when computing maps, the structure of the polarisation pattern changes, and the polarisation looks less aligned. Changes in the polarisation direction are observed in many BSPWNe, and they are usually associated with changes in brightness [44]. Our results suggest that these could originate when the flow decelerates maybe as a consequence of internal shocks, or because of mass loading from the ambient medium.

5. Particle Escape

In few cases, non-thermal high energy emission is observed outside of the supposed location of the contact discontinuity separating the pulsar material from the ISM, where the canonical models predict there should be none. This emission ranges from faint X-ray haloes, as in the case of IC443 [89] and the Mouse [90], or large non-thermal TeV haloes like in the case of Geminga [51, 91], to more structured features like the X-ray *prongs* observed ahead of the bow shock in

G327.1-1.1 [92], or the one sided jets as seen in the Guitar Nebula [93] or in the Lighthouse nebula [94].

Here we illustrate the results obtained by computing the trajectories of high-energy particles in the electric and magnetic field of our simulations, to investigate their possible escape. Results are shown in Fig. 3. The typical energy scale of pairs is set by the condition that their Larmor radius in the equipartition magnetic field in the head is equal to the typical size of the bow-shock [95], and this corresponds, for typical system, to a Lorentz factor $\simeq 3 \times 10^7$.

Our models show a transition in the properties of escaping particles, most of whom comes from the frontal polar region of the pulsar wind, while the others tend to remain confined in the tail. At low energies the escape looks more likely due to reconnection of magnetic field lines between the pulsar wind and ISM: particles moving along those magnetic field lines can escape into the ISM. The outflows are asymmetric (by a factor 4 to 5), likely a consequence of the reconnection at the magnetopause.

At higher energies the escape enters a different regime. It becomes more charge separated. Now current sheets and layers play a more important role, as suggested in [75]. The charge asymmetry is about a factor 1.5, while the spatial asymmetry is a factor 2.

At very high energies the regime becomes fully diffusive [96]: the charge asymmetry exceeds a factor 2, while the spatial asymmetry is reduced to less than 1.5. This transition appears to take place within just an order of magnitude in the energy of the particles from $\gamma = 10^7$ to $\gamma = 10^8$, suggesting that their outflow is quasi-monochromatic.

Both the asymmetry in the escaping flux and it being charge separated, can explain the presence of one-sided jet. Unfortunately the relation between the number of escaping particles and the presence of bright features is non trivial: magnetic field amplification is required, together with turbulent particles confinement, in a non-linear regime [95]. This complex physics goes beyond what we can simulate at the moment. For example, in the presence of a net current, the magnetic field can be amplified more efficiently in the non-resonant regime [97, 98]. This means that self confinement is more efficient.

Our results also show what could be a possible explanation for the X-ray morphology of G327.1-1.1 [92], and the two long tails seen in Geminga [51] (not due to limb brightening).

6. Conclusion

We present here the summary of a detailed numerical study of bow-shock pulsar wind nebulae, carried in 3D using relativistic MHD. Our study was focused on the development of a complete set of models in terms of injection properties, and ISM conditions, that allowed us to investigate not only how the dynamics changes in response to different injections (in terms of spin-axis inclinations, magnetisation, anisotropy) but also to compute on top of these fluid models realistic emission maps, using different prescriptions for the distribution of emitting particles, and to evaluate also the escape properties of high energy pairs, and the possible origin of extended non-thermal features.

Our results show that the large variety of observed morphologies, and structures in known pulsar bow-shocks, can be reasonably well accounted for in terms of differences in the injection conditions. We plan in the future to continue our investigation of few selected configurations, that looks more representative of specific known objects.

6.1. Acknowledgments

We acknowledge the "Accordo Quadro INAF-CINECA (2017-2019)" for high performance computing resources and support. Simulations have been performed as part of the class-A project "Three-dimensional relativistic simulations of bow shock nebulae" (PI B. Olmi). The authors acknowledge financial support from the "Accordo Attuativo ASI-INAF n. 2017-14-H.0

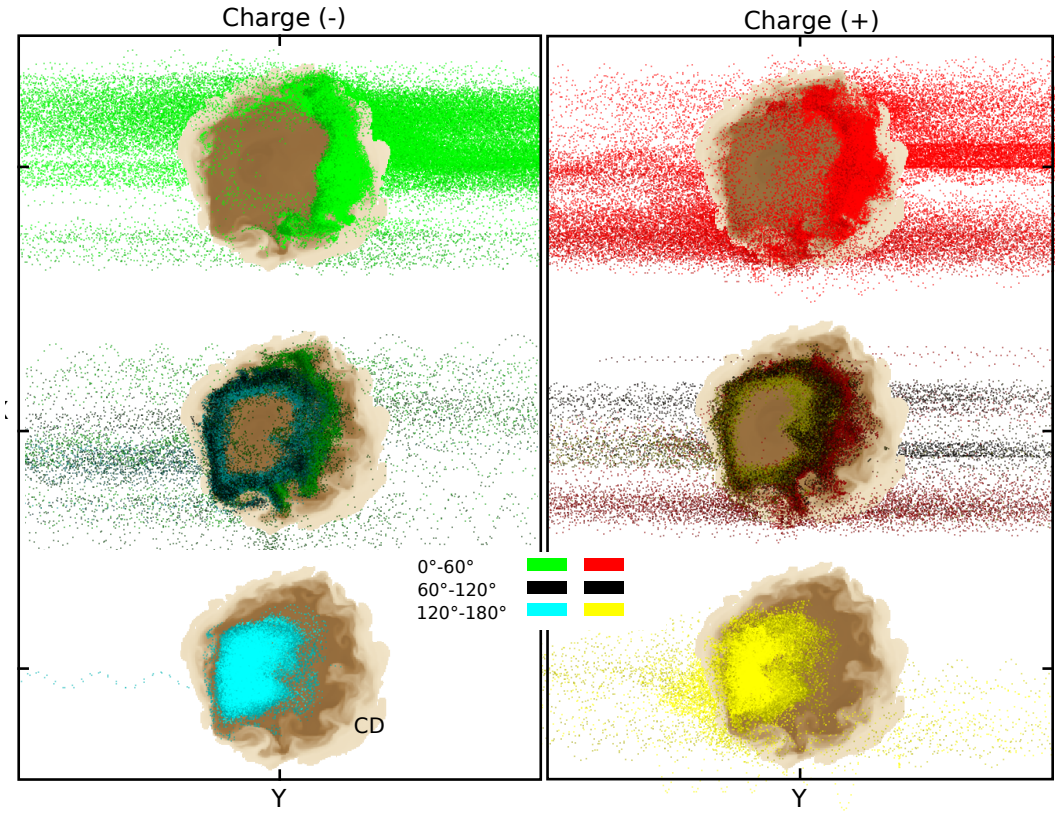

Figure 3. Projection on the plane transverse to the pulsar motion of the 3D-positions of particles injected in the wind with a Lorenz factor $\gamma = 3\times10^7$. Left and right panels refers to particles with different signs. From top to bottom, particles injected within different ranges of the polar angle θ with respect to the pulsar spin-axis: $[0, 60]^\circ$ (green and red) indicates particles injected along the polar current originating from the PSR spin-axis pointing toward the PSR motion, $[60, 120]^\circ$ (black) indicates particles injected along the equatorial current sheet, $[120, 180]^\circ$ (cyan and yellow) indicates particles injected along the polar current pointing in the opposite direction with respect to the PSR motion. The background image shows the $\log_{10}$ cut of the density (darker brown for lower values, lighter brown for higher ones), in the tail at a distance from the pulsar $z = -11.5d_0$ within the position of the contact discontinuity with the ISM material, in order to mark the location of the shocked pulsar wind. From [76].

Progetto: *on the escape of cosmic rays and their impact on the background plasma*" and from the INFN Teongrav collaboration.

References

[1] Gaensler B M and Slane P O 2006 *ARA&A* **44** 17–47 (*Preprint* `arXiv:astro-ph/0601081`)
[2] Bucciantini N 2008 *Advances in Space Research* **41** 491–502 (*Preprint* `arXiv:astro-ph/0702084`)
[3] Olmi B, Del Zanna L, Amato E, Bucciantini N and Mignone A 2016 *Journal of Plasma Physics* **82** 635820601 (*Preprint* `1610.07956`)
[4] Goldreich P and Julian W H 1969 *ApJ* **157** 869–+
[5] Kennel C F and Coroniti F V 1984 *ApJ* **283** 694–709
[6] Kennel C F and Coroniti F V 1984 *ApJ* **283** 710–730
[7] Ruderman M A and Sutherland P G 1975 *ApJ* **196** 51–72

[8] Arons J and Scharlemann E T 1979 *ApJ* **231** 854–879
[9] Contopoulos I, Kazanas D and Fendt C 1999 *ApJ* **511** 351–358 (*Preprint* arXiv:astro-ph/9903049)
[10] Spitkovsky A 2006 *ApJLett* **648** L51–L54 (*Preprint* arXiv:astro-ph/0603147)
[11] Tchekhovskoy A, Philippov A and Spitkovsky A 2016 *MNRAS* **457** 3384–3395 (*Preprint* 1503.01467)
[12] Hibschman J A and Arons J 2001 *ApJ* **560** 871–884 (*Preprint* arXiv:astro-ph/0107209)
[13] Takata J, Wang Y and Cheng K S 2010 *ApJ* **715** 1318–1326 (*Preprint* 1004.1243)
[14] Timokhin A N and Arons J 2013 *MNRAS* **429** 20–54 (*Preprint* 1206.5819)
[15] Takata J, Ng C W and Cheng K S 2016 *MNRAS* **455** 4249–4266 (*Preprint* 1511.06542)
[16] Spitkovsky A 2008 *ApJLett* **682** L5–L8 (*Preprint* 0802.3216)
[17] Sironi L and Spitkovsky A 2009 *ApJLett* **707** L92–L96 (*Preprint* 0908.3193)
[18] Sironi L and Spitkovsky A 2009 *ApJ* **698** 1523–1549 (*Preprint* 0901.2578)
[19] Sironi L, Spitkovsky A and Arons J 2013 *ApJ* **771** 54 (*Preprint* 1301.5333)
[20] Cordes J M and Chernoff D F 1998 *ApJ* **505** 315–338 (*Preprint* astro-ph/9707308)
[21] Arzoumanian Z, Chernoff D F and Cordes J M 2002 *ApJ* **568** 289–301 (*Preprint* astro-ph/0106159)
[22] Sartore N, Ripamonti E, Treves A and Turolla R 2010 *A&A* **510** A23 (*Preprint* 0908.3182)
[23] Verbunt F, Igoshev A and Cator E 2017 *A&A* **608** A57 (*Preprint* 1708.08281)
[24] Truelove J K and McKee C F 1999 *ApJS* **120** 299–326
[25] Cioffi D F, McKee C F and Bertschinger E 1988 *ApJ* **334** 252–265
[26] Leahy D, Green K and Tian W 2014 *MNRAS* **438** 1813–1819
[27] Sánchez-Cruces M, Rosado M, Fuentes-Carrera I and Ambrocio-Cruz P 2018 *MNRAS* **473** 1705–1717 (*Preprint* 1709.07986)
[28] Wilkin F P 1996 *ApJLett* **459** L31
[29] Bucciantini N and Bandiera R 2001 *A&A* **375** 1032–1039
[30] Bucciantini N 2002 *A&A* **387** 1066–1073 (*Preprint* astro-ph/0203504)
[31] Bucciantini N, Amato E and Del Zanna L 2005 *A&A* **434** 189–199 (*Preprint* astro-ph/0412534)
[32] Vigelius M, Melatos A, Chatterjee S, Gaensler B M and Ghavamian P 2007 *MNRAS* **374** 793–808 (*Preprint* astro-ph/0610454)
[33] Barkov M V, Lyutikov M and Khangulyan D 2019 *MNRAS* **484** 4760–4784 (*Preprint* 1804.07327)
[34] Arzoumanian Z, Cordes J, Van Buren D, Corcoran M, Safi-Harb S and Petre R 2004 *AAS/High Energy Astrophysics Division #8* (*Bulletin of the American Astronomical Society* vol 36) p 951
[35] Gaensler B M, van der Swaluw E, Camilo F, Kaspi V M, Baganoff F K, Yusef-Zadeh F and Manchester R N 2004 *ApJ* **616** 383–402 (*Preprint* astro-ph/0312362)
[36] Yusef-Zadeh F and Gaensler B M 2005 *Advances in Space Research* **35** 1129–1136 (*Preprint* astro-ph/0503031)
[37] Li X H, Lu F J and Li T P 2005 *ApJ* **628** 931–937 (*Preprint* astro-ph/0504293)
[38] Gaensler B M 2005 *Advances in Space Research* **35** 1116–1122 (*Preprint* astro-ph/0501357)
[39] Chatterjee S, Gaensler B M, Vigelius M, Cordes J M, Arzoumanian Z, Stappers B, Ghavamian P and Melatos A 2005 *American Astronomical Society Meeting Abstracts* (*Bulletin of the American Astronomical Society* vol 37) p 1470
[40] Kargaltsev O, Misanovic Z, Pavlov G G, Wong J A and Garmire G P 2008 *ApJ* **684** 542-557 (*Preprint* 0802.2963)
[41] Misanovic Z, Pavlov G G and Garmire G P 2008 *ApJ* **685** 1129-1142 (*Preprint* 0711.4171)
[42] Ng C Y, Camilo F, Chatterjee S, Gaensler B M, Yusef-Zadeh F, Hales C, Johnston S, Manchester R N, Kuiper L and van der Swaluw E 2009 *American Astronomical Society Meeting Abstracts #213* (*Bulletin of the American Astronomical Society* vol 41) p 307
[43] Hales C A, Gaensler B M, Chatterjee S, van der Swaluw E and Camilo F 2009 *ApJ* **706** 1316–1322 (*Preprint* 0910.2701)
[44] Ng C Y, Gaensler B M, Chatterjee S and Johnston S 2010 *ApJ* **712** 596–603 (*Preprint* 1002.1815)
[45] De Luca A, Marelli M, Mignani R P, Caraveo P A, Hummel W, Collins S, Shearer A, Saz Parkinson P M, Belfiore A and Bignami G F 2011 *ApJ* **733** 104 (*Preprint* 1102.3278)
[46] Ng C Y, Bucciantini N, Gaensler B M, Camilo F, Chatterjee S and Bouchard A 2012 *ApJ* **746** 105 (*Preprint* 1109.2233)
[47] Marelli M, De Luca A, Salvetti D, Sartore N, Sartori A, Caraveo P, Pizzolato F, Saz Parkinson P M and Belfiore A 2013 *ApJ* **765** 36 (*Preprint* 1212.6664)
[48] Jakobsen S J, Tomsick J A, Watson D, Gotthelf E V and Kaspi V M 2014 *ApJ* **787** 129 (*Preprint* 1404.5059)
[49] Auchettl K, Slane P, Romani R W, Posselt B, Pavlov G G, Kargaltsev O, Ng C Y, Temim T, Weisskopf M C, Bykov A and Swartz D A 2015 *ApJ* **802** 68 (*Preprint* 1501.03225)
[50] Klingler N, Rangelov B, Kargaltsev O, Pavlov G G, Romani R W, Posselt B, Slane P, Temim T, Ng C Y, Bucciantini N, Bykov A, Swartz D A and Buehler R 2016 *ApJ* **833** 253 (*Preprint* 1610.06167)

[51] Posselt B, Pavlov G G, Slane P O, Romani R, Bucciantini N, Bykov A M, Kargaltsev O, Weisskopf M C and Ng C Y 2017 *ApJ* **835** 66 (*Preprint* 1611.03496)
[52] Chevalier R A, Kirshner R P and Raymond J C 1980 *ApJ* **235** 186–195
[53] Kulkarni S R and Hester J J 1988 *Nature* **335** 801–803
[54] Cordes J M, Romani R W and Lundgren S C 1993 *Nature* **362** 133–135
[55] Bell J F, Bailes M, Manchester R N, Weisberg J M and Lyne A G 1995 *ApJLett* **440** L81–L83
[56] van Kerkwijk M H and Kulkarni S R 2001 *A&A* **380** 221–237
[57] Jones D H, Stappers B W and Gaensler B M 2002 *A&A* **389** L1–L5 (*Preprint* astro-ph/0205009)
[58] Brownsberger S and Romani R W 2014 *ApJ* **784** 154 (*Preprint* 1402.5465)
[59] Romani R W, Slane P and Green A W 2017 *ApJ* **851** 61
[60] Rangelov B, Pavlov G G, Kargaltsev O, Durant M, Bykov A M and Krassilchtchikov A 2016 *ApJ* **831** 129 (*Preprint* 1605.07616)
[61] Wang Z, Kaplan D L, Slane P, Morrell N and Kaspi V M 2013 *ApJ* **769** 122 (*Preprint* 1302.6350)
[62] Abeysekara A U e a 2017 *Science* **358** 911–914 (*Preprint* 1711.06223)
[63] Blasi P and Amato E 2011 *ArXiv:1007.4745* (*Preprint* 1007.4745)
[64] Amato E and Blasi P 2017 *ArXiv e-prints* (*Preprint* 1704.05696)
[65] Bucciantini N 2002 *A&A* **393** 629–635 (*Preprint* astro-ph/0207016)
[66] Morlino G, Lyutikov M and Vorster M 2015 *MNRAS* **454** 3886–3901 (*Preprint* 1505.01712)
[67] Olmi B, Bucciantini N and Morlino G 2018 *MNRAS* (*Preprint* 1809.03807)
[68] Bandiera R 1993 *A&A* **276** 648 (*Preprint* astro-ph/9305004)
[69] van der Swaluw E, Achterberg A, Gallant Y A, Downes T P and Keppens R 2003 *A&A* **397** 913–920 (*Preprint* astro-ph/0202232)
[70] Bucciantini N 2017 *MNRAS* **471** 4885–4893 (*Preprint* 1709.00885)
[71] Barkov M V, Lyutikov M, Klingler N and Bordas P 2019 *MNRAS* **485** 2041–2053 (*Preprint* 1804.07341)
[72] Olmi B and Bucciantini N 2019 *MNRAS* **484** 5755–5770 (*Preprint* 1902.00442)
[73] Olmi B and Bucciantini N 2019 *MNRAS* **488** 5690–5701 (*Preprint* 1907.12356)
[74] Bucciantini N 2018 *MNRAS* **478** 2074–2085 (*Preprint* 1805.01653)
[75] Bucciantini N 2018 *MNRAS* **480** 5419–5426 (*Preprint* 1808.08757)
[76] Olmi B and Bucciantini N 2019 *MNRAS* **490** 3608–3615 (*Preprint* 1910.01926)
[77] Mignone A and McKinney J C 2007 *MNRAS* 473–+
[78] Mignone A, Striani E, Tavani M and Ferrari A 2013 *MNRAS* ***in press.*** (*Preprint* 1309.0375)
[79] Miyoshi T and Kusano K 2005 *Journal of Computational Physics* **208** 315–344
[80] Mignone A and Bodo G 2006 *MNRAS* **368** 1040–1054 (*Preprint* astro-ph/0601640)
[81] Olmi B, Del Zanna L, Amato E and Bucciantini N 2015 *MNRAS* **449** 3149–3159 (*Preprint* 1502.06394)
[82] Del Zanna L, Volpi D, Amato E and Bucciantini N 2006 *A&A* **453** 621–633 (*Preprint* astro-ph/0603080)
[83] Volpi D, Del Zanna L, Amato E and Bucciantini N 2007 *Mem.SAIt* **78** 662
[84] Bucciantini N, del Zanna L, Amato E and Volpi D 2005 *A&A* **443** 519–524 (*Preprint* astro-ph/0508212)
[85] Olmi B, Del Zanna L, Amato E, Bandiera R and Bucciantini N 2014 *MNRAS* **438** 1518–1525 (*Preprint* 1310.8496)
[86] Boris J P and Shanny R A 1972 Proceedings : fourth conference on numerical simulation of plasmas (november 2-3, 1970)
[87] Vay J L 2008 *Physics of Plasmas* **15** 056701
[88] Higuera A V and Cary J R 2017 *Physics of Plasmas* **24** 052104 (*Preprint* 1701.05605)
[89] Swartz D A, Pavlov G G, Clarke T, Castelletti G, Zavlin V E, Bucciantini N, Karovska M, van der Horst A J, Yukita M and Weisskopf M C 2015 *ApJ* **808** 84 (*Preprint* 1506.05507)
[90] Gaensler B M, van der Swaluw E, Camilo F, Kaspi V M, Baganoff F K, Yusef-Zadeh F and Manchester R N 2004 *ApJ* **616** 383–402 (*Preprint* astro-ph/0312362)
[91] Abeysekara A U, Albert A, Alfaro R, Alvarez C, Álvarez J D, Arceo R, Arteaga-Velázquez J C, Avila Rojas D, Ayala Solares H A, Barber A S, Bautista-Elivar N, Becerril A, Belmont-Moreno E, BenZvi S Y, Berley D, Bernal A, Braun J, Brisbois C, Caballero-Mora K S and Capistrán T 2017 *Science* **358** 911–914 (*Preprint* 1711.06223)
[92] Temim T, Slane P, Kolb C, Blondin J, Hughes J P and Bucciantini N 2015 *ApJ* **808** 100 (*Preprint* 1506.03069)
[93] Hui C Y and Becker W 2007 *A&A* **467** 1209–1214 (*Preprint* astro-ph/0610505)
[94] Pavan L, Bordas P, Pühlhofer G, Filipović M D, De Horta A, O'Brien A, Balbo M, Walter R, Bozzo E, Ferrigno C, Crawford E and Stella L 2014 *A&A* **562** A122 (*Preprint* 1309.6792)
[95] Bandiera R 2008 *A&A* **490** L3–L6 (*Preprint* 0809.2159)
[96] Bykov A M, Amato E, Petrov A E, Krassilchtchikov A M and Levenfish K P 2017 *Space Sci. Rev.* **207** 235–290 (*Preprint* 1705.00950)

[97] Skilling J 1971 *ApJ* **170** 265
[98] Bell A R 2004 *MNRAS* **353** 550–558